Design Optimization of Spar Floating Wind Turbines Considering Different Control Strategies

Design Optimization of Spar Floating Wind Turbines Considering Different Control Strategies

John Marius Hegseth[1], **Erin E. Bachynski**[1], **Joaquim R. R. A. Martins**[2]

[1] Department of Marine Technology, NTNU, 7491 Trondheim, Norway
[2] Department of Aerospace Engineering, University of Michigan, Ann Arbor, MI 48109, USA

E-mail: john.m.hegseth@ntnu.no

Abstract. One of the challenges related to the design of floating wind turbines (FWTs) is the strong interactions between the controller and the support structure, which may result in an unstable system. Several control strategies have been proposed to improve the dynamic behaviour, all of which result in trade-offs between structural loads, rotor speed variation, and blade pitch actuator use, which makes controller design a challenging task. Due to the interactions, simultaneous design of the controller and support structure should be performed to properly identify and compare different solutions. In the present work, integrated design optimization of the blade-pitch controller and support structure is performed for a 10 MW spar FWT, considering four different control strategies, to evaluate the effect of the controller on the structural design and associated costs. The introduction of velocity feedback control reduces the platform pitch response and consequently the fatigue loads in the tower, which leads to a decrease in the tower costs compared to a simple PI controller. Low-pass filtering of the nacelle velocity signal to remove the wave-frequency components results in reduced rotor speed variation, but offers only small improvements in costs, likely due to the limited wave-frequency response for the considered designs. Comparisons with nonlinear time-domain simulations show that the linearized model is able to capture trends with acceptable accuracy, but that significant overpredictions may occur for the platform pitch response.

1. Introduction

For floating wind turbines (FWTs), the performance of the control system generally depends on the support structure design and vice versa. A well-known interaction between the blade pitch controller and platform motions is the introduction of negative damping above rated wind speed [1]. While detuning the controller gains such that the bandwidth is reduced achieves stability, this results in poorer rotor speed tracking performance [1, 2]. Several alternative methods have also been suggested to resolve the issue, such as introducing a feedback term proportional to the pitch velocity [3] or nacelle velocity [4, 5] to manipulate the generator speed reference. For these types of feedback control, Fleming et al. [6] also suggested to remove the wave-frequency components from the velocity signal, as this reduced the tower loads. All of these control strategies result in trade-offs between structural loads, rotor speed variation, and blade pitch actuator use, which vary with different environmental conditions. Therefore, identifying optimal control parameters is a challenging task.

Due to the strong interactions, simultaneous design of the controller and support structure should be performed to have a fair comparison between different solutions. A step toward simultaneous design was made by Lemmer et al. [7], who optimized the main dimensions of a three-column semi-submersible FWT. They minimized a combination of material costs and damage-equivalent loads in the tower for seven operational conditions, with a constraint on the static pitch angle at rated thrust. The controller was tuned at each design iteration using a linear quadratic regulator (LQR) approach. To properly identify and compare optimal solutions, the integrated control and structural designs should, however, be evaluated over the lifetime of the system, considering actual design limits. The purpose of the present study is to perform integrated design optimization of the blade-pitch controller and support structure for

a 10 MW FWT, considering long-term fatigue damage and extreme response constraints, to evaluate the effect of different control strategies on the structural design and associated costs.

2. Linearized FWT dynamics

2.1. FWT definition

The present study perfoms the design optimization of a spar buoy that supports the DTU 10 MW reference wind turbine [8] at a water depth of 320 m. The steel hull is partially filled with concrete ballast to achieve the correct draft, using a ballast density of 2600 kg/m^3. The interface with the tower is located 10 m above the still water line (SWL), while the hub height is 119 m above the SWL. A catenary mooring system consisting of three lines spread symmetrically about the vertical axis is used for station-keeping. Only the response in the xz-plane is considered in the current work, and co-directional waves and wind travelling in the positive x-direction are applied in all simulations. An overview of the FWT system is shown in Fig. 1.

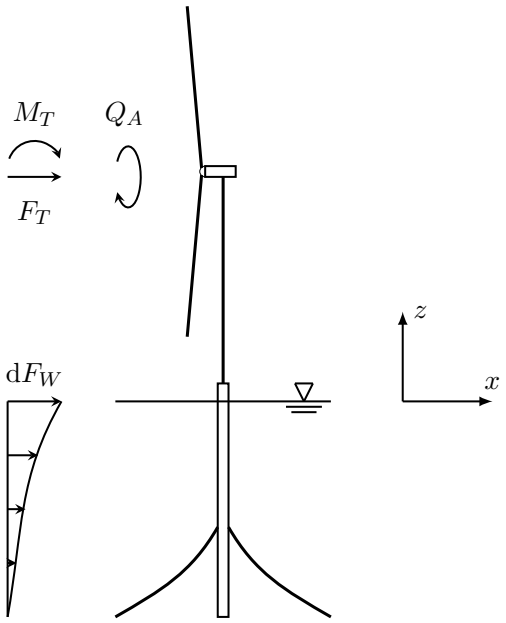

Figure 1: Overview of the FWT system.

2.2. Linearized equations of motion

The system is linearized and expressed in state-space form, and consists of a structural part and a control system part, which are connected to obtain the complete closed-loop aero-hydro-servo-elastic model as described by Hegseth et al. [9]. For each wind-wave condition, the operational point is found from static equilibrium when the system is subjected to the mean wind loads. The linearized system considers perturbations in the state and input variables, $\mathbf{x}$ and $\mathbf{u}$ respectively, about the operational point:

$$\mathbf{x} = \mathbf{x_0} + \Delta\mathbf{x}, \quad \mathbf{u} = \mathbf{u_0} + \Delta\mathbf{u}. \tag{1}$$

The dynamic equations of motion are then expressed as

$$\Delta\dot{\mathbf{x}} = \mathbf{A}\Delta\mathbf{x} + \mathbf{B}\Delta\mathbf{u}, \tag{2}$$

where $\mathbf{A}$ is the state matrix and $\mathbf{B}$ is the input matrix.

2.3. Structural model

The structural model for the platform and turbine considers four degrees-of-freedom (DOFs), namely surge, pitch, first tower/platform bending mode, and rotor speed. The equations of motions for the former three are found from generalized displacements similar to Hegseth and Bachynski [10], but using a flexible hull to ensure a correct natural frequency for the first bending mode, while a rigid drivetrain and rotor is assumed for the rotor dynamics. The structural state vector is thus written as

$$\mathbf{x}_s = \begin{bmatrix} \xi_1 & \xi_5 & \xi_7 & \dot{\xi}_1 & \dot{\xi}_5 & \dot{\xi}_7 & \dot{\varphi} \end{bmatrix}^\top, \tag{3}$$

where ξ_n represents generalized support structure DOF n, and $\dot{\varphi}$ is the rotor speed.

Hydrodynamic excitation loads on the hull are described by MacCamy–Fuchs theory, and transverse added mass is based on analytical 2D coefficients. Radiation damping is neglected, while viscous damping is found from stochastic linearization of the drag term in Morison's equation.

Wind loads on the rotor are derived from linearized BEM theory with the incoming wind field described by the Kaimal spectrum and an exponential coherence function for the longitudinal wind

velocity component [11]. The blades are considered rigid in the model, and the aerodynamic forces on the rotor are applied as resultant loads at the tower top. In addition, the static component of the aerodynamic quadratic drag force on the tower is included.

The inputs to the structural system consist of both control system outputs and disturbances due to environmental loads. The control input vector contains the references for the generator torque (Q_G) and the collective blade pitch angle (θ), and is defined as

$$\mathbf{u}_{sc} = [Q_G \quad \theta]^\top . \tag{4}$$

The disturbance vector contains rotor-effective wind speeds for thrust, tilting moment and aerodynamic torque, and generalized wave excitation forces for each support structure DOF, i.e.

$$\mathbf{u}_{sd} = [v_{F_T} \quad v_{M_T} \quad v_{Q_A} \quad F_{W,1} \quad F_{W,5} \quad F_{W,7}]^\top . \tag{5}$$

2.4. Controller description

The baseline linear control system consists of a generator-torque controller and a collective blade-pitch controller, which work independently in below-rated and above-rated wind speeds, respectively. Below rated wind speed, the generator torque is set to be proportional to the square of the rotor speed to maintain the optimal tip-speed ratio. Above rated wind speed, the generator torque is kept constant, and four different strategies are considered for the blade-pitch controller:

- CS1: Gain-scheduled PI controller
- CS2: Gain-scheduled PI controller + platform pitch velocity feedback
- CS3: Gain-scheduled PI controller + nacelle velocity feedback
- CS4: Gain-scheduled PI controller + nacelle velocity feedback + low-pass filter

For feedback control using platform pitch or nacelle velocity, we use the modified rotor speed reference, $\dot{\varphi}_0'$, defined by Lackner [3]:

$$\dot{\varphi}_0' = \dot{\varphi}_0(1 + k_f \dot{x}_f) \tag{6}$$

where $\dot{\varphi}_0$ is the nominal rotor speed reference, k_f is the velocity feedback gain, and $\dot{x}_f$ is either the platform pitch velocity or the nacelle velocity. An updated expression for the rotor speed error can then be established as

$$\Delta\dot{\varphi}' = \dot{\varphi} - \dot{\varphi}_0' = \Delta\dot{\varphi} - \dot{\varphi}_0 k_f \dot{x}_f, \tag{7}$$

where $\Delta\dot{\varphi}$ is the nominal rotor speed error. In CS4, the nacelle velocity signal is passed through a first order low-pass filter to remove the wave-frequency components before it is fed back to the blade-pitch controller.

2.5. Response calculations

The structural and control system models are written as a single closed-loop system, which is solved in the frequency domain. Dynamic force equilibrium is then used together with the response spectra to calculate the bending moment response along the tower.

The fatigue damage is calculated at selected locations in the tower using the Dirlik method [12], while the extreme response of the support structure is found using the AUR method, where the most probable maximum value in one hour is used in the design constraints. The model has earlier been verified against fully coupled nonlinear time domain simulations in SIMA [9].

The rotor speed tracking performance is evaluated using the weighted average of the rotor speed standard deviation, which is found by summing the values from each short-term condition that is considered, weighted by their associated probabilities:

$$\sigma_{(\dot{\varphi})} = \sum_{i=1}^{N_{EC}} p_i \sigma_{(\dot{\varphi}),i}. \tag{8}$$

Here, N_{EC} is the number of short-term conditions, $\sigma_{(\dot{\varphi}),i}$ is the rotor speed standard deviation in condition i, and p_i is the probability of the condition.

To evaluate blade-pitch actuator fatigue, the actuator duty cycle (ADC) was defined in Kendall et al. [13] as the total number of degrees pitched divided by the total simulation time. Although ADC cannot be used as an absolute measure of the actuator fatigue damage, it is suitable for comparison of different control strategies. The normalized ADC, which is used in the current work, is defined by Bottasso et al. [14] as

$$\mathrm{ADC}_i = \frac{1}{T}\int_0^T \frac{|\dot{\theta}_i(t)|}{\dot{\theta}_{\max}}\mathrm{d}t, \tag{9}$$

where $\dot{\theta}_i$ is the blade pitch rate in condition i, T is the total simulation time, and $\dot{\theta}_{\max}$ is the maximum allowable blade pitch rate, which for the DTU 10 MW is equal to 10 deg/s.

If the process is ergodic, the ADC can be expressed using the expected value:

$$\mathrm{ADC}_i = \frac{1}{\dot{\theta}_{\max}} E\left[|\dot{\theta}_i(t)|\right]. \tag{10}$$

Assuming that the blade pitch rate is Gaussian, the expected value can be calculated as

$$E\left[|\dot{\theta}_i(t)|\right] = \sqrt{\frac{2}{\pi}}\sigma_{(\dot{\theta}),i}. \tag{11}$$

For the linearized model, the ADC can thus be derived from the blade pitch rate standard deviation. The weighted average ADC used in the design optimization is then found similarly as in Eq. (8).

2.6. Environmental conditions

Fifteen different ECs are used to evaluate the long-term fatigue performance in the present work. The conditions span mean wind speeds from 1-30 m/s with 2 m/s step, and for each mean wind speed, the most probable values for the significant wave height and spectral peak period are used. These values, as well as the associated probabilities of occurrence, are found from the joint probability distribution derived by Johannessen et al. [15], and shown in Fig. 2.

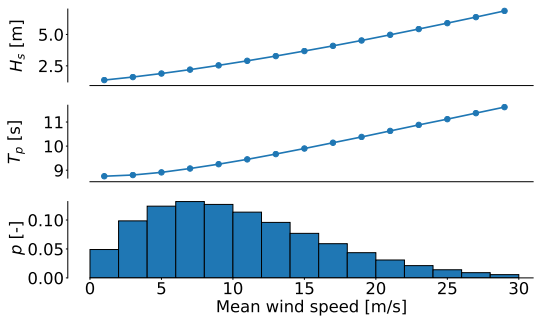

Figure 2: Significant wave heights, spectral peak periods, and normalized probabilities applied in the fatigue calculations.

Three ECs, described in Table 1, along the 50-year contour surface, are selected to evaluate the extreme response. EC 1 and 2 represent operational wind speeds above rated, while EC 3 considers an extreme storm condition, where the turbine is parked with feathered blades. For all ECs, the IEC Class B normal turbulence model (NTM) [11] is used for the incoming wind, while the waves are described by a JONSWAP spectrum with a peakedness parameter of 3.3.

3. Optimization problem

The FWT model is implemented in OpenMDAO [16], which is an open-source framework for multidisciplinary design, analysis, and optimization. The design is optimized using a gradient-based approach, where the derivatives of the model are computed analytically using coupled adjoints. The optimization problem is solved using the SNOPT algorithm [17], which uses a sequential quadratic programming (SQP) approach, through the pyOptSparse Python interface [18].

3.1. Objective function

The objective function used in the present work is the combined cost of the platform and tower, C_{spar} and C_{tower} respectively:

$$f = C_{\mathrm{spar}} + C_{\mathrm{tower}}. \tag{12}$$

Table 1: Environmental conditions for extreme response calculations.

Condition	1	2	3
Mean wind speed at hub height, U (m/s)	13.0	21.0	50.0
Significant wave height, H_s (m)	8.1	9.9	15.1
Spectral peak period, T_p (s)	14.0	15.0	16.0
Turbulence intensity at hub height, I (-)	0.17	0.14	0.12

The costs consider both material and manufacturing, using the cost models developed by Farkas and Jármai [19]. Costs related to installation, maintenance, and decommissioning are not included. The cost of the platform (and similarly of the tower) is expressed as

$$C_{spar} = k_m M_{\text{spar}} + k_f \sum_i T_i, \tag{13}$$

where k_m is the steel cost factor, M_{spar} is the steel mass of the hull, and k_f is the fabrication cost per unit time. T_i is the time spent at fabrication stage i, expressed as a function of the geometry. The steel cost factor, k_m, is assumed to have a value of 2.7 €/kg, while the ratio between the material and fabrication cost factors, k_m/k_f, is set to 1.0, which is a typical value for West European labour [19]. The cost of the concrete ballast is neglected in the current work.

3.2. Design variables

Both the platform and tower are discretized into ten sections along the length. For the tower, the diameter and wall thickness at the nodes connecting the sections are set as design variables. The length of the tower sections is kept fixed during the optimization, to maintain the original hub height.

The structural design of the spar platform is primarily governed by buckling loads, which for most parts of the hull are dominated by the hydrostatic pressure. The structural design of the platform is therefore not considered in the study, and only the diameter at the platform nodes and the length of each section are included in the design optimization. The wall thickness is expressed as a function of depth, based on the optimized structural design from Hegseth et al. [9]. This ensures a proper mass distribution, and penalizes designs with large drafts and consequently high external pressure loads, which require increased use of material. The mooring system design is kept fixed during the optimization.

For the control system, the optimization considers the proportional (k_p) and integral (k_i) gains for the blade-pitch controller, as well as the velocity feedback gain (k_f) for the pitch and nacelle velocity feedback control. For CS4, the corner frequency of the nacelle velocity low-pass filter (ω_f) is also included.

3.3. Constraints

The fatigue damage at each tower node is evaluated using an SN curve approach, where the D curve in air from DNV-RP-C203 [20] is applied together with a design fatigue factor (DFF) of 2.0 [21], and the lifetime of the FWT system is chosen to be 20 years. The fatigue design constraints are thus expressed as

$$D_{tot} = N_{20} \sum_{i=1}^{N_{\text{EC}}} p_i D_i \leq \frac{1.0}{\text{DFF}}, \tag{14}$$

where D_{tot} is the total fatigue damage in 20 years, N_{20} is the number of short term conditions in 20 years, and D_i is the fatigue damage in condition i.

Tower buckling is assessed using Eurocode 3 [22], assuming that the tower is stiffened between each section to reduce the buckling length. To ensure a smooth transition between the platform and tower, the tower base diameter is set to be equal to the diameter at the platform top. Both fatigue and buckling constraints are aggregated using Kreisselmeier–Steinhauser (KS) functions [23].

The maximum platform pitch angle in the considered 50-year conditions is limited to 15 . Although the heave response is not included in the model, heave resonance in the wave frequency range is avoided by placing a lower limit of 25 s on the heave natural period. The added mass in heave is approximated as the value for a 3D circular disc with the same diameter as the platform bottom [24].

The presented model is valid strictly for hull sections with vertical walls, and a maximum taper angle of 10° is therefore applied as a constraint for each section of the platform, to avoid shapes where the physics are not captured correctly. Offset constraints are not considered, as the surge response is mostly governed by the rotor and mooring system design.

Appropriate upper limits for the rotor speed variation and blade-pitch actuator use are difficult to quantify. The constraints are therefore based on values taken from the land-based DTU 10 MW wind turbine with the original controller [25], where the weighted average rotor speed standard deviation and ADC are found from nonlinear time domain analyses using the simulation tool SIMA. Initial analyses found that the rotor speed variation obtained with the land-based turbine was unrealistic for the floating system with the simplified controllers considered in the present work. To enlarge the feasible region of the design space, the constraints for both the rotor speed variation and the ADC are scaled by a factor of 1.5 compared to the land-based values, as shown in Table 2.

4. Results

4.1. Optimized designs

The optimized support structure design for CS1 is illustrated in Fig. 3. The hourglass shape taken by the platform below the wave zone increases the distance between the center of buoyancy and the center of gravity, which leads to increased pitch restoring stiffness, while the relatively large diameter at the bottom results in larger added mass and consequently longer natural period in heave. For the upper part of the platform and intersection with the tower, the optimizer finds a balance between a small diameter, which is desirable with regards to hydrodynamic loads, and a large diameter, which (together with a small wall thickness) is the most cost-effective way to achieve the required fatigue life.

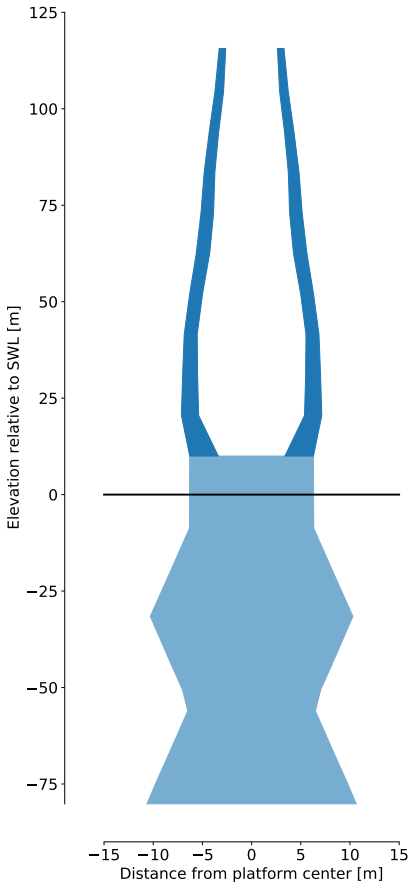

Figure 3: Optimized support structure design for CS1. The wall thickness in the tower is scaled by a factor of 40 relative to the diameter for illustration purposes.

The optimized tower diameter and wall thickness distributions for the different control strategies are plotted in Fig. 4. All four solutions follow the same trends, and the effect of velocity feedback control is most visible for the wall thickness, where the values for CS2-4 are approximately 20 % lower than for the simple PI controller (CS1) along most of the tower length. The reduced wall thickness is enabled by a decrease in the fatigue loads for these controllers, which is the design-driving constraint for the tower. For all four control strategies, the 15° pitch angle constraint is also active; however, as the 50-year storm condition with parked turbine (EC3) is found to be the critical load case for extreme response, this constraint is not affected by the controller.

The improved fatigue performance can be understood by examining the response spectra for the optimized designs. In Fig. 5a, the tower base bending moment spectra are shown for a mean wind speed of 15 m/s. Large differences are seen around the pitch natural frequency at 0.15 rad/s, where the velocity feedback controllers increase the aerodynamic damping and thus reduce the response. The low-pass filtering of the nacelle velocity removes the wave-frequency range from the signal, which results in a higher optimal velocity feedback gain and nearly eliminates the tower base bending moment response

Table 2: Land-based and applied constraint values for the rotor speed variation and blade-pitch actuator use.

Variable	Land-based value	Constraint value
$\sigma_{(\dot{\varphi})}$ [rad/s]	4.22E-2	6.33E-2
ADC [-]	5.10E-3	7.65E-3

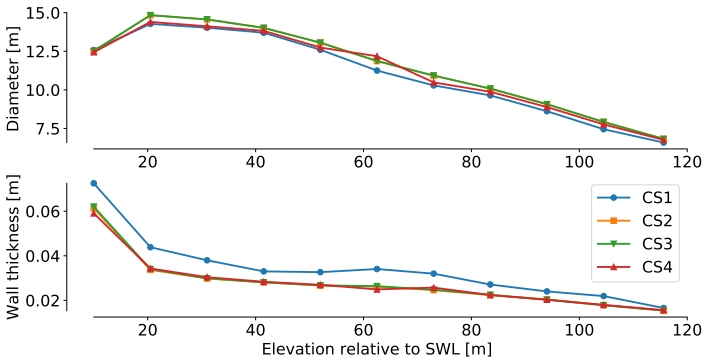

Figure 4: Tower diameter and wall thickness for optimized designs.

arising from resonant pitch motions. The wave-frequency bending moments, on the other hand, is unaffected by the control strategy. The blade pitch spectra in Fig. 5b show how the larger PI gains in the velocity feedback controllers result in overall increased actuator use, with the exception of the pitch natural frequency, as well as the wave-frequency band for CS4.

The optimized costs of the tower, platform, and tower plus platform for CS2-4 are shown in Fig. 6a, compared to the optimized costs for CS1. The majority of the cost reductions come from the tower, due to the improved fatigue behaviour, whereas the platform is less affected due to the fixed costs related to buckling resistance and the 15° pitch angle constraint. However, because a lighter tower results in a lower overall center of gravity, the platform pitch response is somewhat improved, and a small reduction in platform costs of about 2 % is also observed. Because the platform accounts for 70-75 % of the total costs for the considered designs, the resulting total cost reduction is approximately 6 %.

The resulting rotor speed standard deviations and ADCs, normalized by their maximum allowable values from Table 2, are shown in Fig. 6b. For each control strategy, there exists a limit where no further reduction in cost can be achieved by increasing the actuator use. This limit is higher for the velocity feedback controllers than for a controller using only the rotor speed error as input, which causes the ADC constraint to be inactive at the optimum for CS1. A larger ADC may result in higher probability of fatigue failure for the actuator bearings, and therefore more detailed design considering the lifetime of the system should be performed to determine appropriate values for this constraint.

For the rotor speed variation, better performance is achieved with CS4 than with the other control strategies. Since there is a trade-off between rotor speed variation and structural loads (and thus costs) as previously discussed, it is expected that larger cost reductions can be achieved with CS4 if the rotor speed constraint is tightened.

Some limitations to this work should be noted. The standard deviation in steady-state conditions is used as the only measure of the rotor speed tracking performance, and extreme rotor speed excursions due to gusts are not considered. The effect of the controllers on surge motions, drivetrain response, mooring line tension, or blade response has also not been studied. In addition, the performance of the FWT system could likely be further improved by also adding individual pitch control or modifications to the torque controller, which have not been examined in the present work.

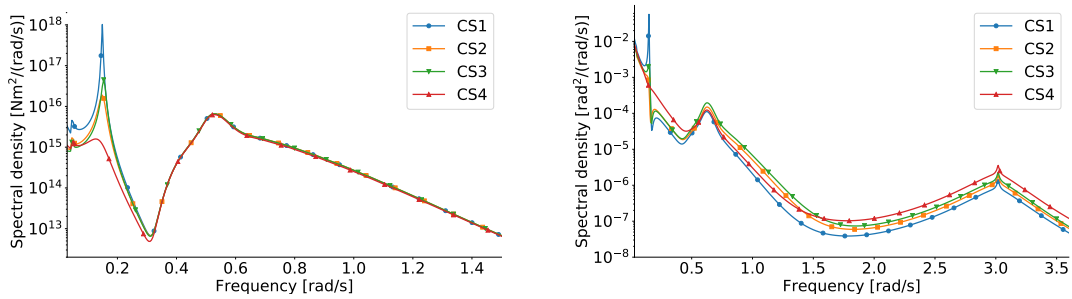

(a) Tower base bending moment. **(b)** Blade pitch.

Figure 5: Response spectra, 15 m/s mean wind speed.

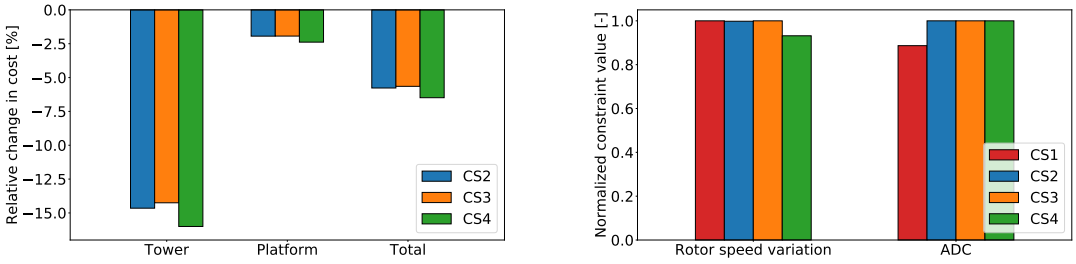

(a) Costs relative to CS1. **(b)** Rotor speed variation and ADC values.

Figure 6: Objective and constraint function values for optimized designs.

4.2. Sequential versus multidisciplinary optimization

In the presented methodology, the platform, tower, and blade-pitch controller are optimized simultaneously. This approach, commonly known as multidisciplinary design optimization (MDO) [26], is preferred for coupled systems, where a sequential optimization process in general leads to suboptimal solutions on the overall system level [27]. To assess the importance of integrated design, results using MDO are compared to a sequential optimization for CS4, where the controller and support structure are optimized separately. For the sequential approach, the control parameters are first optimized to minimize the rotor speed variation, with constraints on system stability and ADC. All support structure parameters are kept constant and structural constraints are not considered. The support structure is then optimized for minimum cost, keeping the controller parameters fixed at their optimized values from the previous step. This procedure is repeated until the system has converged. Since this method results in different objective functions for the two sequential problems, a multi-objective approach is utilized for the MDO study, where a combination of costs and rotor speed variation is minimized with different relative weighting.

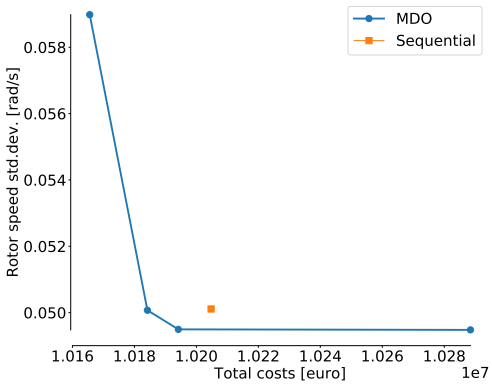

Figure 7: MDO vs. sequential optimization.

Figure 7 shows the MDO Pareto front together with the optimal solution from the sequential approach. The results confirm that improved designs can be achieved with integrated optimization; however, the differences are small. For the same rotor speed variation, using MDO results in

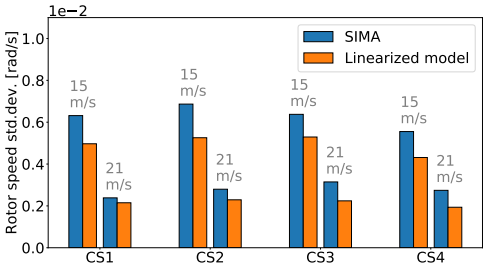

(a) Weighted rotor speed variation.

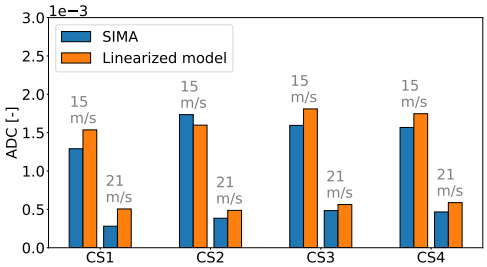

(b) Weighted ADC.

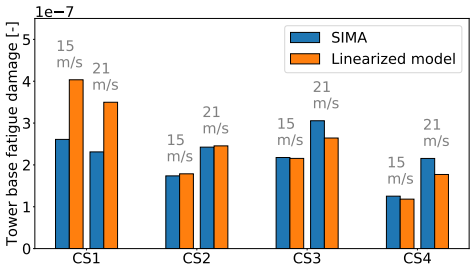

(c) Weighted tower base 1-h fatigue damage.

Figure 8: Comparison of response parameters with SIMA.

approximately 0.5 % reduction in the costs of the tower, or 0.2 % in total costs. Although small coupling effects are seen for the considered optimization problem, larger differences are expected in cases where the controller has a greater effect on the structural response.

4.3. Verification

The optimized controller designs are verified through fully coupled nonlinear time-domain simulations using SIMA, where two different ECs above rated wind speed are simulated with each control strategy for a specified support structure design. Comparisons with the linearized model for different response parameters, weighted by the probability of each condition, are shown in Fig. 8.

The linearized model is seen to mostly follow the trends observed in the nonlinear simulations, but some errors are present. The largest errors are observed for the tower base fatigue damage, which is significantly overestimated for CS1, whereas good agreement is obtained with the other control strategies. The reason for the poor agreement is that the aerodynamic (and thus the overall) damping for the platform pitch mode is much lower with this control strategy. Consequently, the resonant pitch response becomes very sensitive to the presence and amount of additional damping in the system, which is either not considered or underpredicted in the linear model. This disagreement was also observed for a linearized model of the 10 MW OO-Star semisubmersible in Souza et al. [28], which used a control strategy similar to CS1. The overestimation of fatigue damage means that the optimized tower design for CS1 is more conservative than for the other control strategies, suggesting that the cost reductions in Fig. 6a are highly optimistic, and that CS1 may yield a fatigue design similar to that with a nacelle velocity feedback controller. It also suggests that future optimization studies using the linearized model should consider more advanced control strategies than CS1, to limit the pitch response error.

In addition, the rotor speed standard deviation is consistently underestimated by about 20 % for all four control strategies. This disagreement could be taken into consideration in the optimization process by adjusting the constraint value.

5. Concluding remarks

The design of the platform, tower, and blade-pitch control system for a 10 MW spar FWT was optimized simultaneously using a linearized aero-hydro-servo-elastic model and gradient-based optimization with

analytic derivatives. The goal has been to minimize the material and manufacturing costs of the support structure, with constraints on tower fatigue damage and buckling, extreme platform pitch motions, rotor speed variation, and blade-pitch actuator use, considering four different strategies for the blade-pitch controller.

The effect of the controller on the structural response was limited to the fatigue damage in the tower, since the storm condition with parked turbine was found to govern the extreme responses of the system considered here. The reduction in tower loads for the velocity feedback controllers compared to the simple PI control system was a consequence of lower platform pitch response, which led to a reduction in the wall thickness required to satisfy the long-term fatigue damage constraint. Consequently, the tower costs were reduced, and also the platform costs due to better dynamic performance. Although low-pass filtering of the nacelle velocity signal did not offer significant cost reductions, this control strategy also saw a reduction in rotor speed variation, since the constraint was inactive at the optimum. It is also expected that the effect of this filter will be more prominent for FWT concepts with larger wave-frequency response.

Comparisons with nonlinear time-domain simulations showed that the linearized model in general is able to capture trends with acceptable accuracy, but that the platform pitch response can be significantly overpredicted for designs with low aerodynamic damping if contributions from other sources of damping are small. This was the case for CS1, which indicates that the cost reductions achieved for CS2-4 are considerably overestimated. For the velocity feedback controllers, which increases the amount of aerodynamic damping induced by the control system, this problem was not observed, and good agreement was achieved.

The presented approach is useful for conceptual FWT design, where it can be used to quickly explore the design space before resorting to higher fidelity tools for detailed subsystem analysis and design. The model captures important interactions between the controller and support structure, and enables assessment of trade-off effects in a lifetime perspective. Further, the methodology can be extended to account for additional design parameters and load cases, which may help identify novel design solutions.

References

[1] T. J. Larsen and T. D. Hanson. “A Method to Avoid Negative Damped Low Frequent Tower Vibrations for a Floating, Pitch Controlled Wind Turbine”. In: *Journal of Physics: Conference Series* 75 (2007), p. 012073.

[2] J. Jonkman. “Influence of Control on the Pitch Damping of a Floating Wind Turbine”. In: *46th AIAA Aerospace Science Meeting and Exhibit, Reno, Nevada*. 2008.

[3] M. Lackner. “Controlling Platform Motions and Reducing Blade Loads for Floating Wind Turbines”. In: *Wind Engineering* 33.6 (2009), pp. 541–553.

[4] G. J. van der Veen, I. J. Couchman, and R. O. Bowyer. “Control of floating wind turbines”. In: *2012 American Control Conference, Fairmont Queen Elizabeth, Montreal, Canada*. 2012, pp. 3148–3153.

[5] P. A. Fleming et al. “Evaluating Methods for Control of an Offshore Floating Turbine”. In: *Proceedings of the ASME 2014 33rd International Conference on Ocean, Offshore and Arctic Engineering (OMAE2014), San Francisco, California, USA*. 2014.

[6] P. A. Fleming, A. Peiffer, and D. Schlipf. “Wind Turbine Controller to Mitigate Structural Loads on a Floating Wind Turbine Platform”. In: *Journal of Offshore Mechanics and Arctic Engineering* 141 (2019).

[7] F. Lemmer et al. “Optimization of Floating Offshore Wind Turbine Platforms With a Self-Tuning Controller”. In: *Proceedings of the ASME 2017 36th International Conference on Ocean, Offshore and Arctic Engineering (OMAE2017), Trondheim, Norway*. 2017.

[8] C. Bak et al. *Description of the DTU 10 MW Reference Wind Turbine*. Tech. rep. DTU Wind Energy Report-I-0092. DTU Wind Energy, 2013.

[9] J. M. Hegseth, E. E. Bachynski, and J. R. R. A. Martins. “Integrated design optimization of spar floating wind turbines”. In: *Marine Structures* 72 (2020).

[10] J. M. Hegseth and E. E. Bachynski. "A semi-analytical frequency domain model for efficient design evaluation of spar floating wind turbines". In: *Marine Structures* 64 (2019), pp. 186–210.

[11] IEC. *Wind Turbines - Part 1: Design Requirements*. Tech. rep. IEC 61400-1. 2005.

[12] T. Dirlik. "Application of Computers in Fatigue Analysis". PhD thesis. University of Warwick, 1985.

[13] L. Kendall et al. "Application of Proportional-Integral and Disturbance Accommodating Control to Variable Speed Variable Pitch Horizontal Axis Wind Turbines". In: *Wind Engineering* 21.1 (1997), pp. 21–38.

[14] C. L. Bottasso et al. "Optimization-based study of bend-twist coupled rotor blades for passive and integrated passive/active load alleviation". In: *Wind Energy* 16 (2013), pp. 1149–1166.

[15] K. Johannessen, T. S. Meling, and S. Haver. "Joint Distribution for Wind and Waves in the Northern North Sea". In: *International Journal of Offshore and Polar Engineering* 12.1 (2002), pp. 1–8.

[16] J. S. Gray et al. "OpenMDAO: An open-source framework for multidisciplinary design, analysis, and optimization". In: *Structural and Multidisciplinary Optimization* 59 (2019), pp. 1075–1104.

[17] P. E. Gill, W. Murray, and M. A. Saunders. "SNOPT: an SQP Algorithm for Large-Scale Constrained Optimization". In: *SIAM Journal on Optimization* 12.4 (2002), pp. 979–1006.

[18] R. E. Perez, P. W. Jansen, and J. R. R. A. Martins. "pyOpt: A Python-Based Object-Oriented Framework for Nonlinear Constrained Optimization". In: *Structural and Multidisciplinary Optimization* 45.1 (2012), pp. 101–118.

[19] J. Farkas and K. Jármai. *Optimum Design of Steel Structures*. Springer, 2013.

[20] DNV. *Fatigue Design of Offshore Steel Structures*. Tech. rep. DNV-RP-C203. 2010.

[21] DNV. *Design of Floating Wind Turbine Structures*. Tech. rep. DNV-OS-J103. 2013.

[22] European Committee for Standardization. *Eurocode 3: Design of Steel Structures, Part 1-6: Strength and Stability of Shell Structures*. Tech. rep. EN 1993-1-6: 2007. 2007.

[23] G. Kreisselmeier and R. Steinhauser. "Systematic Control Design by Optimizing a Vector Performance Index". In: *International Federation of Active Controls Symposium on Computer-Aided Design of Control Systems, Zurich, Switzerland*. 1979.

[24] DNV. *Modelling and Analysis of Marine Operations*. Tech. rep. DNV-RP-H103. 2011.

[25] M. H. Hansen and L. C. Henriksen. *Basic DTU Wind Energy controller*. Tech. rep. DTU Wind Energy Report-E-0018. 2013.

[26] J. R. R. A. Martins and A. B. Lambe. "Multidisciplinary Design Optimization: A Survey of Architectures". In: *AIAA Journal* 51.9 (2013), pp. 2049–2075.

[27] M. Muskulus and S. Schafhirt. "Design optimization of wind turbine support structures-A review". In: *Journal of Ocean and Wind Energy* 1.1 (2014), pp. 12–22.

[28] C. E. S. Souza, J. M. Hegseth, and E. E. Bachynski. "Frequency-dependent aerodynamic damping and inertia in linearized dynamic analysis of floating wind turbines". In: *Journal of Physics: Conference Series* 1452.012040 (2020).